Scientific Report 2013-2015

Ideas program. Exploratory research projects

Implementation of project Cod PN-II-ID-2012-4-0028:
Alkali and silver halides based magnetic tunnel junctions
December 2014 – December 2015

2015 Year Report

Objectives:

I. Fe/LiBr(001) and Fe/LiF(001) junctions

II. Fe/NaBr/Fe(001) interfaces

III. Double perovskites based on calcium

Results: publication of two or three papers in ISI quoted reviews. Presentation of one paper at International Conference.

1. Fe/LiBr(001) and Fe/LiF(001) magnetic tunnel junctions

The ground states electronic and magnetic properties of Fe(001)semi-infinite Fe(001)/nFe/mLiF(LiBr)/nFe(001) semi-infinite heterojunctions were studied by using a first-principles, scalar-relativistic and spin-polarized surface Green's function technique (SGF) implemented within the tight-binding linear muffin –tin orbital (TB-LMTO) method in the atomic sphere approximation (ASA), together with the coherent potential approximation (CPA), in order to describe the disorder effects like the intermixing at interfaces. The spin-resolved ballistic conductances in the current-perpendicular-to-plane (CPP) geometry, at zero-temperature and zero-bias, have been evaluated within the TB-LMTO-CPA Kubo-Landauer formalism and including the vertex corrections. The tunneling magnetoresistance ratios are express by the asymmetry of the conductances between FM and AFM configurations of Fe electrodes normalized to AFM one, $TMR = (\sigma_{FM}-\sigma_{AFM})/\sigma_{AFM}$.

The bcc structure was considered for Fe electrodes and rocksalt structure for LiF and LiBr. Calculations are performed for lattice parameters, epitaxially fixed at the lattice spacing of bulk iron, $a_{LiBr}=2a_{Fe}$, $a_{LiF} = \sqrt{2}a_{Fe}$. Two models interfaces are considered in the present calculations with Fe atoms located above Li sites and Fe atoms located above F(Br) atoms – Fig.I.1. The atomic monolayers are counted from interfaces. Due to open structure of LiF, to fulfill ASA space filling requirement, two empty spheres (ES) at interstices positions Fe/LiF(LiBr)/Fe)(100) interface, were added. Fe was located atop of F.

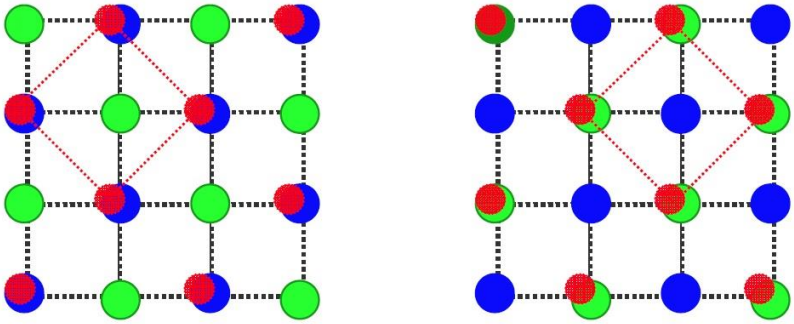

IC_{Fe-F} IC_{Fe-Br}

Fig.I.1

The interface stability has been analysed. As example, in Fig.I.2, the data obtained in case of Fe/LiF/Fe(001) interface is plotted. The most stable is the IC_{Fe-F} one, with Fe atoms located atop of F ones. Stable interfaces were also evidenced when Fe atoms are located both above Li and Br sites in case of Fe/LiBr/Fe(001) heterostructure.

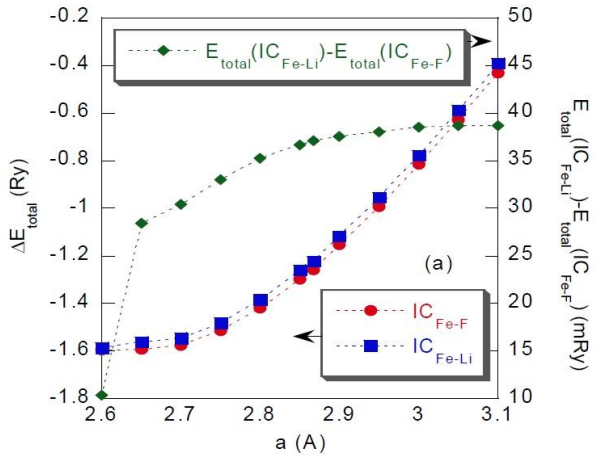

Fig.I.2

The interface stability has been studied, at IC_{Fe-F} one, as effect of mixing. The intermixing is described by $Fe_2(Fe_1)_{1-x}F_x/F_{1-x}Fe_xLi$ and $Fe_2(Fe)_{1-x}Li_x/Li_{1-x}Fe_xF$. For F-Fe interdiffusion, the total energy, E_{tot}(AFM,FM), increases up to x = 0.6 and then decreases. For Li-F interdiffusion, the E_{tot}(AFM,FM) increases. As result of F interdiffusion (interstitial), E_{tot}(FM,AFM) decreases for $x < 0.5$ and then increases, while for Li interdiffusion (interstitial) E_{tot}(FM,AFM) increases up to x = 0.6, then decreasing. At IC_{Fe-Li} interface, the intermixing is described by: $Fe_2(Fe_1)_{1-x}F_x/Fe_{1-x}Fe_xLi$ and $Fe_2(Fe_1)_{1-x}Li_x/Li_{1-x}Fe_xF$ relations. The total energy decreases for both FM and AFM configurations at $x < 0.5$, in case of Fe interdiffusion (interstitial), while E_{tot} increases both for AFM and FM configurations in case of F interdiffusion (Li-F intermixing), Fe interdiffusion (F-Fe intermixing) at $x \leq 0.6$ and Li interdiffusion (interstitial) at $x < 0.5$.

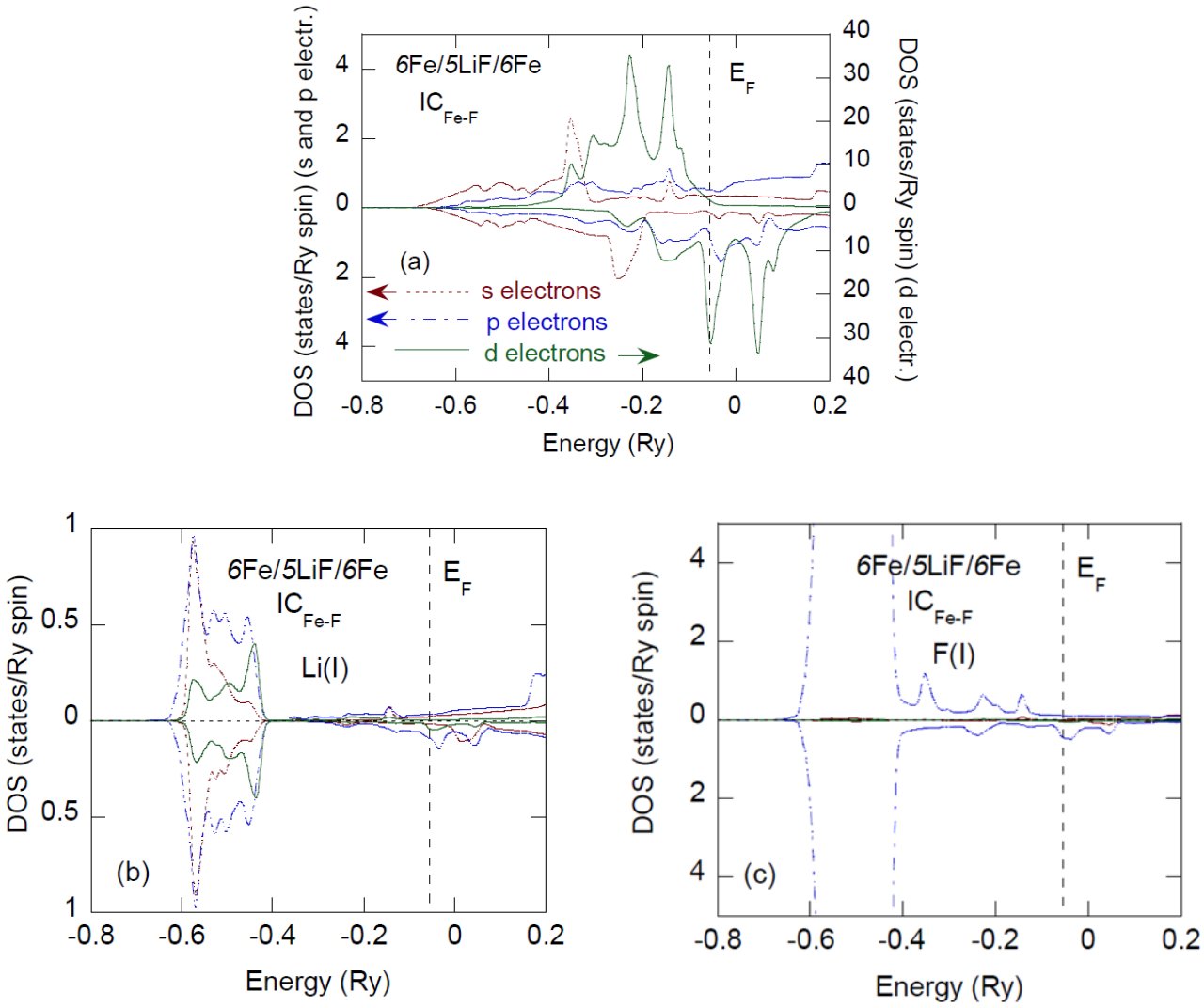
6Fe/5LiF/6Fe
IC Fe-F
E F
(a)
s electrons
p electrons
d electrons
DOS (states/Ry spin) (s and p electr.)
DOS (states/Ry spin) (d electr.)
Energy (Ry)
Li(I)
(b)
F(I)
(c)

Fig.I.3a

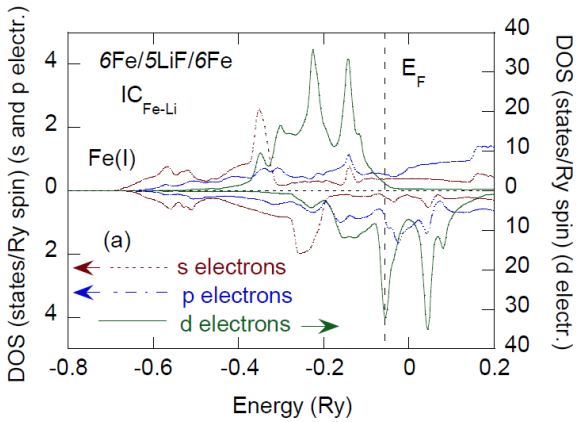
6Fe/5LiF/6Fe
IC Fe-Li
E F
Fe(I)
(a)
s electrons
p electrons
d electrons
DOS (states/Ry spin) (s and p electr.)
DOS (states/Ry spin) (d electr.)
Energy (Ry)

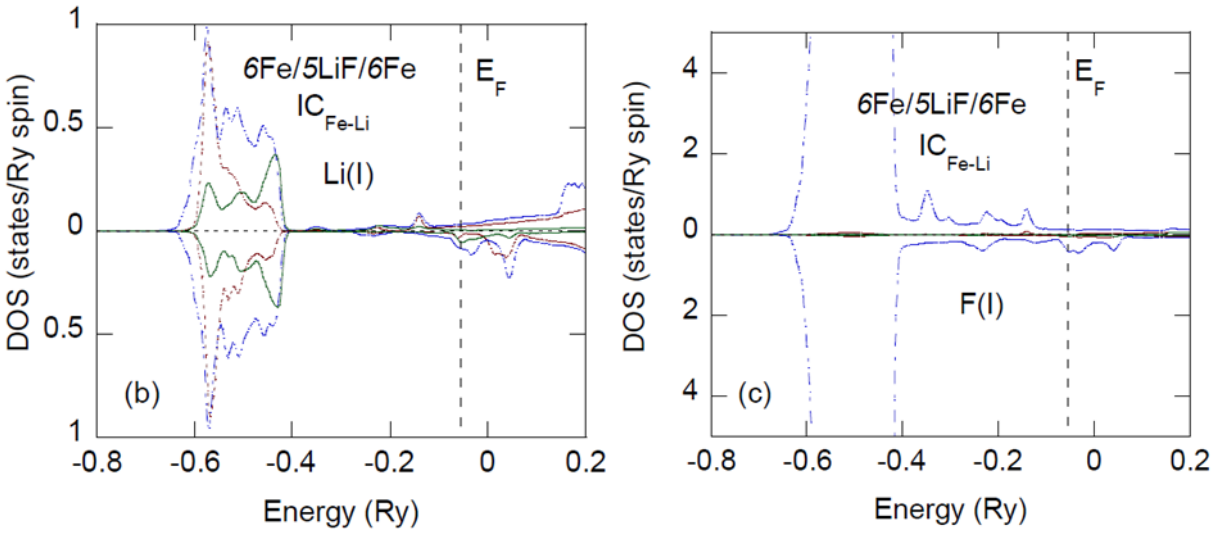

Fig.I.3b

Layer- and atom-resolved spin-polarized density of states (DOS) of 6Fe/5LiF/6Fe heterostructures, with IC_{Fe-F} and IC_{Fe-Li} model interfaces, were studied. The l-resolved DOS of interfacial Fe, F and Li atoms are given in Fig.I.3. As result of interactions between Fe and LiF(LiBr) interfacial layers, in the energy range of the band gap of bulk LiF(LiBr), iron induced gap states (MIGs) are evidenced, in both barriers, near interfaces. The induced states appear on both Li and F ions making Fe/LiF(001) interfaces practically metallic. When departing from interfaces, the semiconducting character of the barriers tends to be recovered. At IC_{Fe-F} interfaces the majority-spin MIGs, around E_F, result mostly from s-electrons of cationic sites and p-electrons at anionic positions. The minority-spin MIGs are more localized and show a peak around E_F mainly due to p- and d-electrons. At IC_{Fe-Li} interface, the largest contributions to minority-spin MIGs have predominatly a conduction band character for Li ions and a valence band character for F ions, whilst the majority-spin MIGs have a rather valence character for both ions.

The charge transfer and the magnetization profiles of 6Fe/5LiF/6Fe heterostructures are given in Fig.I.4. Due to the location of iron Fermi level near the bothom of the LiF conduction band, there is a charge transfer between Fe magnetic slabs and LiF spacers. As result of the charge transfer at interfaces, the formation of MIGs in the band gap of barrier is evidenced. At IC_{Fe-F} interface, the charge transfer of Fe(I) is -0.46 e^- and at IC_{Fe-Li} one of -0.41 e^-. There is a charge modulation in the interfacial iron layers. On the barrier side there is a decrease of F charge and an increase of Li charge at both analysed interfaces. The interfacial iron magnetic moments are enhanced over the bulk one, their values being of M_{Fe}=2,85 μ_B (IC_{Fe-F}) and M_{Fe}=2,81 μ_B (IC_{Fe-Li}). Small positive polarizations are induced on F and Li – Fig.I.4.

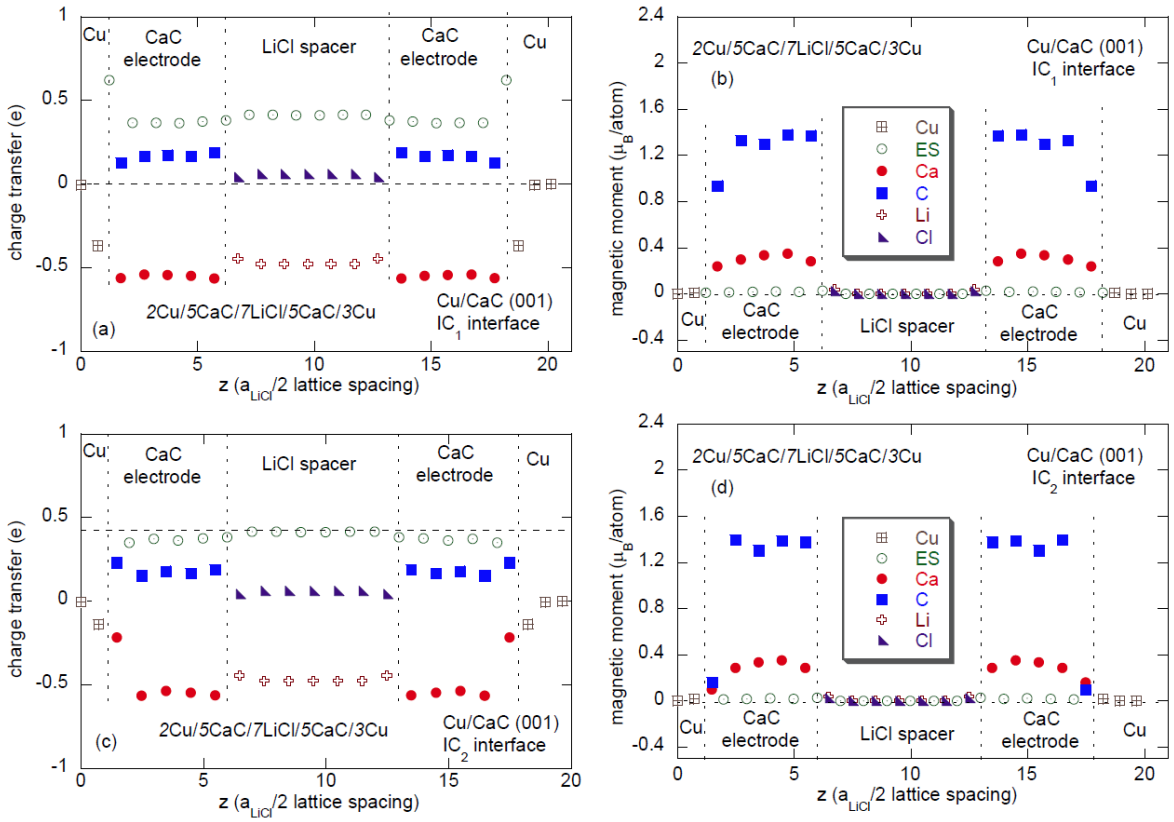

Fig.I.4

The interlayer exchange couplings, as function of the barrier thicknesses, for 6Fe/mLiF/6Fe and 6Fe/mLiBr/6Fe heterostructures were analysed. In case of LiF barrier, there is no exchange coupling, while for LiBr barrier there is a small ferromagnetic coupling, decreasing exponentially with barrier thickness.

The spin resolved FM(AFM) conductances and TMR ratios of 6Fe/mLiF/6Fe(001) heterostructures having $IC_{Fe\text{-}F}$ and $IC_{Fe\text{-}Li}$ configurations are given in Fig.I.5, while in Fig.I.6, the data obtained for Fe/nLiBr/Fe heterostructures are plotted. In case of LiF barrier, the largest contributions, at both interfaces, are due to FM conductances with spin down electrons. These conductances decrease exponentially with barrier thickness. High TMR values (≅ 2000 %) are evidenced in case of $IC_{Fe\text{-}Li}$ interface configuration. Somewhat different behaviour is evidenced in case of LiBr barrier. The largest contribution, as above, is given by FM conductance with spin down electrons. In this case a change of slope is evidenced at n = 11. There is a high increase of the TMR ratio at n = 11. For higher barrier thickness the TMR values are nearly constant, having a value ≅ $3.2 \cdot 10^4$%.

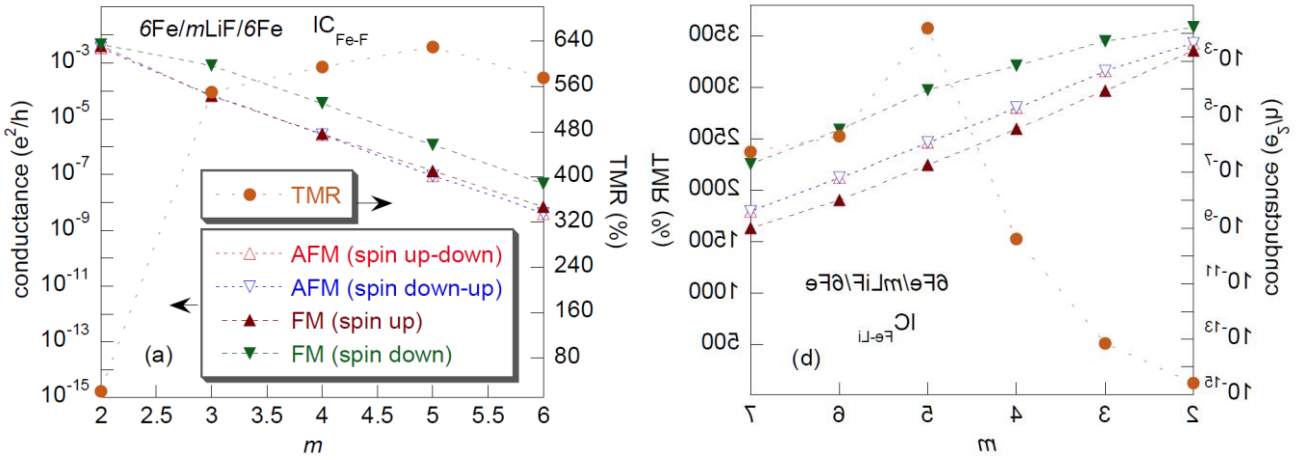

Fig.I.5

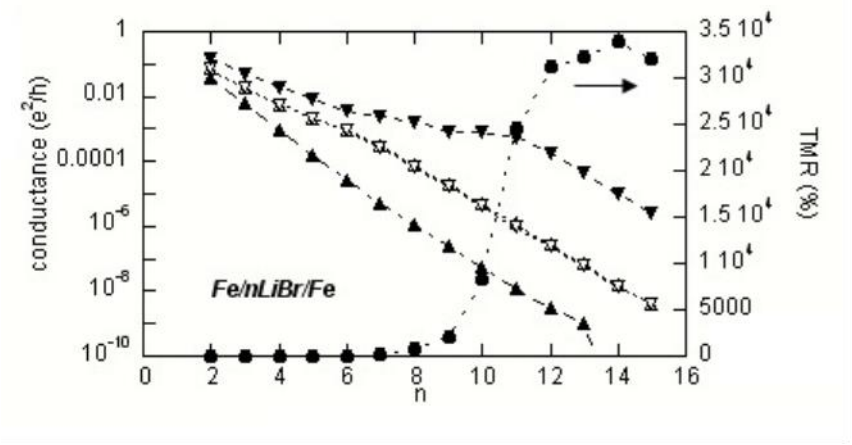

Fig.I.6

The $\mathbf{k}_{\parallel}$-resolved partial conductances of 6Fe/5LiF/6Fe heterostructure, for $IC_{Fe\text{-}F}$ and $IC_{Fe\text{-}Li}$ interface configurations, are given in Fig.I.7. For both heterojunctions the majority-spin FM conductances are free-electron like with a broad peak and very large transmissions maxima at $\bar{\Gamma}$ point. At the interface the wave vector split in $k_{\parallel}$ which is conserved during the scattering and k_z along the transmission direction. Inside the barrier gap, k_z becomes complex $k_z = q+i$ where the imaginary part i describes the exponential decay of the corresponding evanescent states. The transmission probability, T, for a given $k_{\parallel}$, decreases exponentially with the, barrier thickness, d $T \propto \exp(-2kd)$,. These data confirm the tunneling mechanism across the LiF and LiBr barriers.

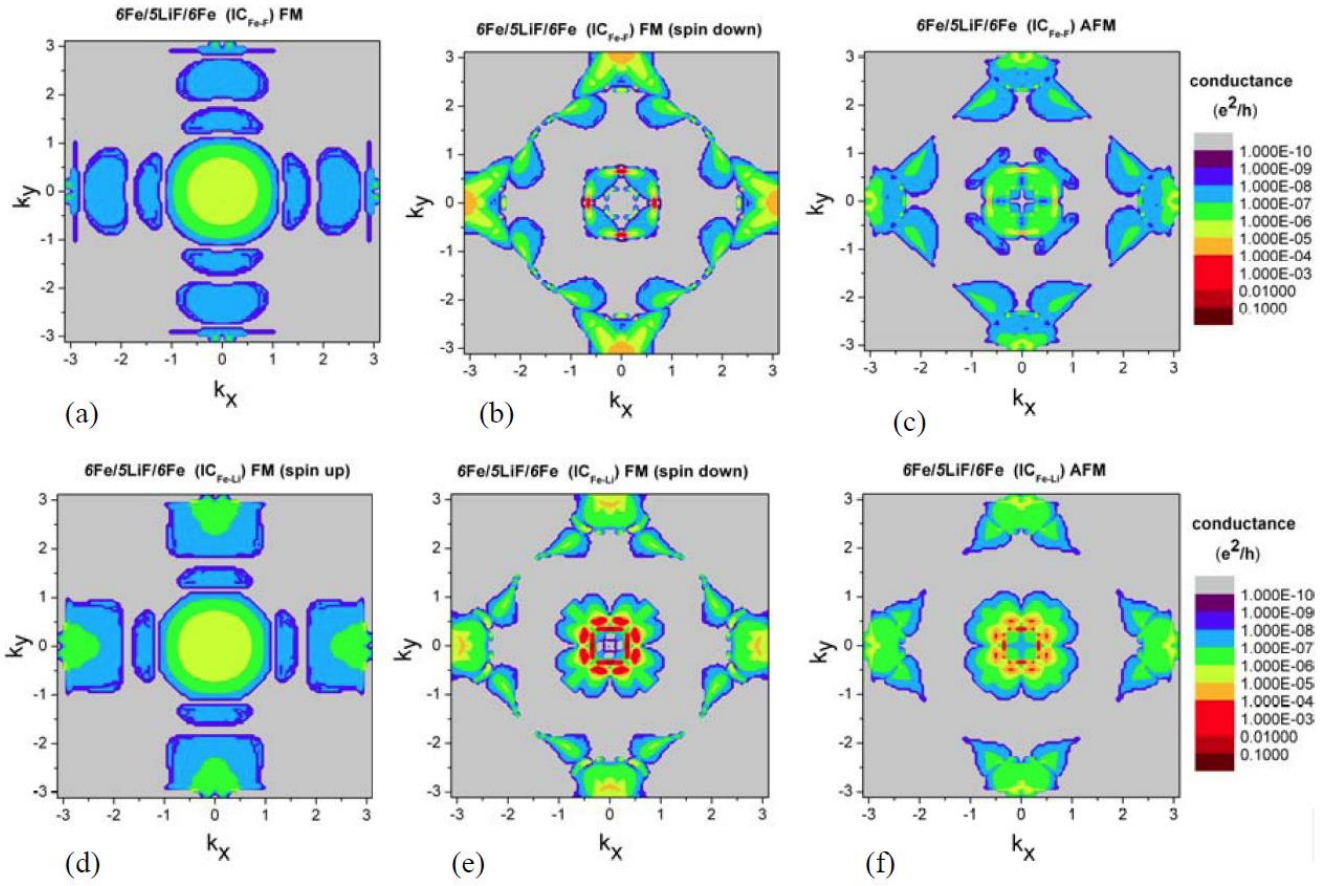

Fig.I.7

The effects of interdiffusion at the Fe/LiF/Fe interfaces were studied. For both F-Fe and Li-Fe intermixing, the TMR values decrease up to an exchange level x = 0,15 and then becomes nearly constant.

The scientific results obtained on the above heterostructures have been presented at International Conference (invited lecture) and also sent for publication.

1.1 ***Electronic properties of Fe/LiF(LiBr)/Fe magnetic tunnel junctions***

E.Burzo, P.Vlaic

The 15th international Balkan Workshop on Applied Physics, 2-4 July 2015, SO-02, Invited lecture. SO-02

1.2 ***Are insulating LiF barriers relevant for spin-polarized tunneling applications? Insight from first-principles***

E.Burzo, P. Vlaic, C.Karva

Journal Phys. D:Appl. Phys. (will be send for publication)

II. Heterojunctions of CaC/MgS/CaC type; Fe/NaBr/Fe(01) interfaces

II.1 CaC/MgS/CaC heterostructures

Preliminary results on CaC/MgS/CaC(001) tunnel junctions were presented at TIM 14 Conference on Physics. Since this system showed very interesting properties, we decided to continue the study of the

system and to publish the results in a top scientific journal. There are many additional data on this system as compared with the previous ones; some of them will be presented in the following.

The analyses of the electronic structure and magnetic properties of rocksalt monocarbide, CaC, show that it that is stable, nearly half-metallic and ferromagnetic. The spin-polarized band structure of the rocksalt-type CaC compound (fat bands) with equilibrium lattice spacing of 5.20 Å is plotted in Fig.II.1. The determined magnetic moment is of 1.82 μ_B/f.u.. There is a negative Fermi level spin polarization of 50 %. The Curie temperatures have been evaluated at T_c = 779 K for the compound with B1-type structure and T_c=1412 K for B3-type one, both exceeding room temperature one. The total energy calculations performed on MgS compound predict the presence of B1-type phase with equilibrium lattice spacing of ≅ 5.15 Å, only by 1 % smaller than the experimental value, of 5.2033 Å. The calculated band structures and the density of states are given in Fig.II.2. MgS is predicted to be an indirect Γ-X band gap semiconductor with the top of the valence band at the Γ_{15} point and the bottom of the conduction band at the X_1 point. The calculated band gap is of 0.206 Ry, somewhat lower than the experimental one.

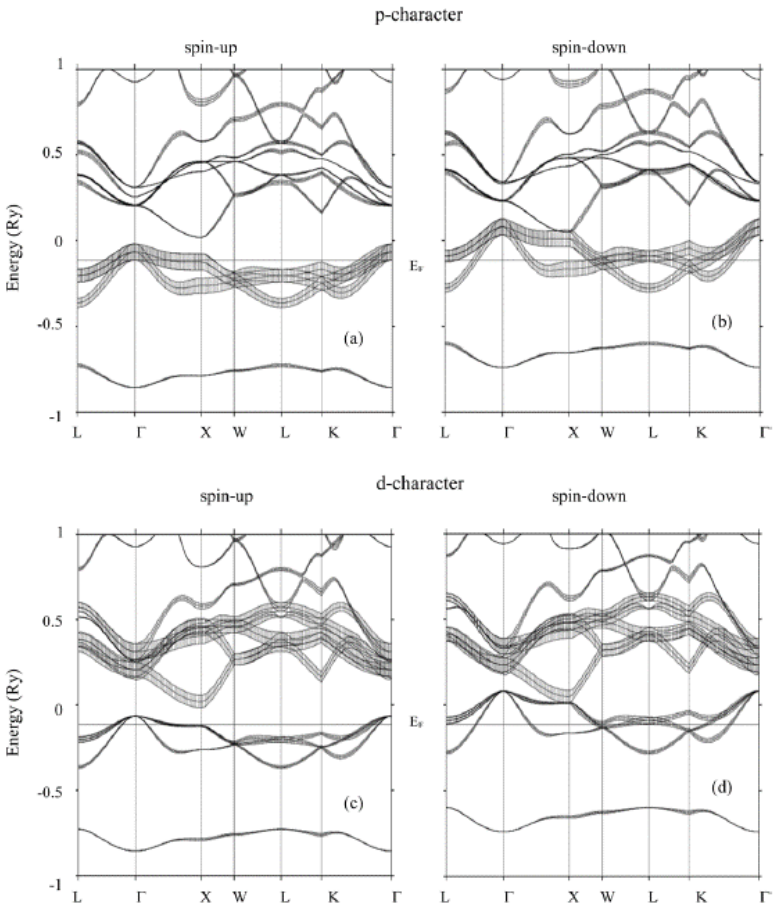

Fig.II.1

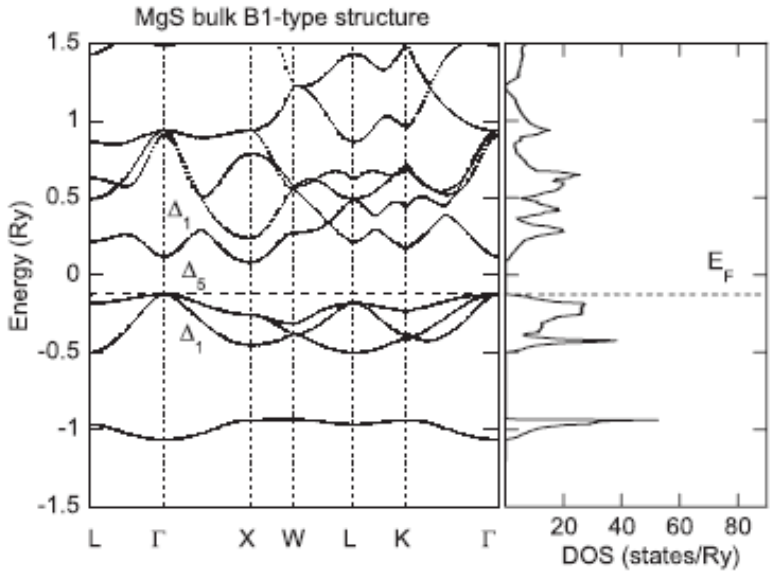

Fig.II.2

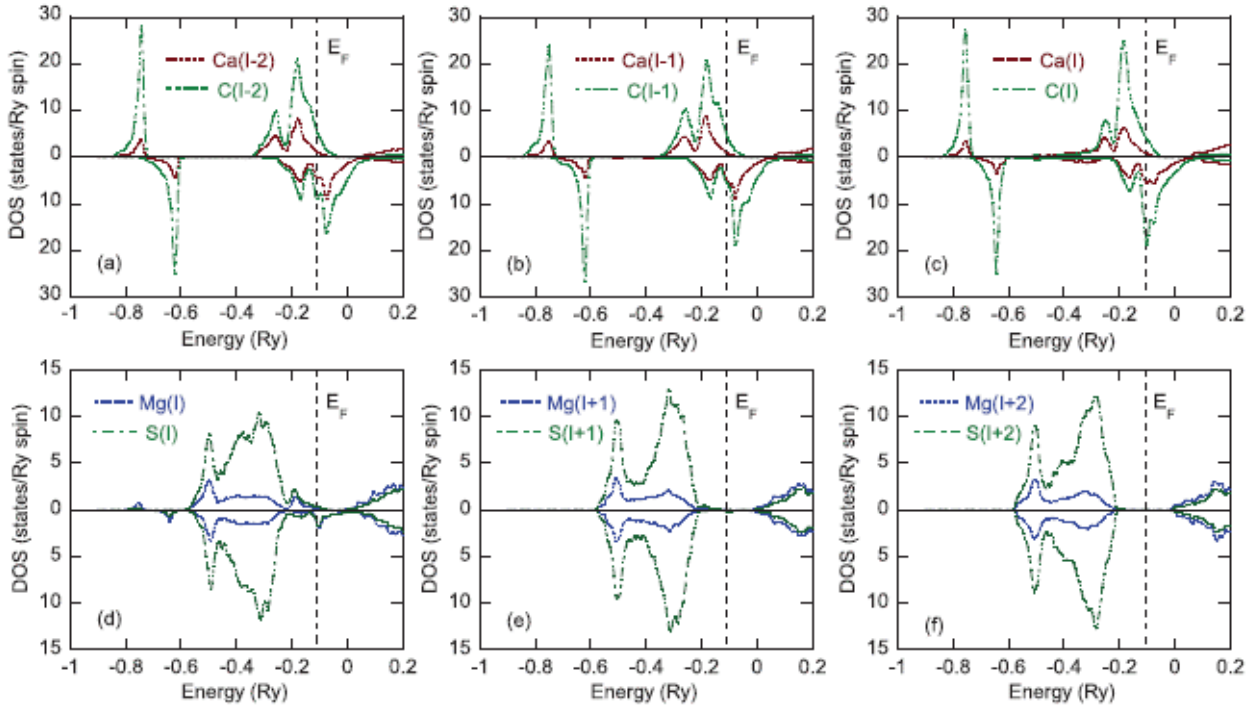

Fig.II.3

The 2Cu/5CaC/nMgS/5CaC/5Cu(001) heterostructures were further analysed. Their layer and atom-resolved DOS is given in Fig.II.3, for CaC(I-2), CaC(I-1) and CaC(I) layers as well as for MgS(I), MgS(I+1) and MgS(I+2) layers. When departing form the CaC/MgS(001) and Cu/CaC(001) interfaces, toward the middle of the CaC slabs, the DOS of CaC layers exhibits a bulk-like behaviour with almost fully occupied majority-spin sub-bands and the peak in the minority spin DOS, located at E_F. At the cost of a small reduction in the exchange splitting between the majority- and minority-spin valence subbands of the interfacial C atoms, the spin polarization at E_F, $P(E_F)$ increases up to 63 % in the interfacial CaC

layers – Fig.II.3c. Near the CaC/MgS(001) interfaces, in the region corresponding to the band gap of bulk MgS, the presence of induced gap states on both Mg and S ions as well as a closure of the MgS band gap are evidenced – Fig.II.3d. The Fermi level spin-polarization, induced on the interfacial MgS(I) monolayer is negative and has a value of 80 %.

According to the bulk CaC electronic structure , along the Δ direction, Δ_1 state are present at the E_F in both spin channels, while Δ_5 states are only present in the majority-spin sub-band. However, at CaC/MgS(001) interfaces, the majority – and minority-spin sub-bands are shifted to lower energies and both Δ_1 and Δ_5-states contribute to conduction process in both spin channels – Fig.II.4a,b. The tunneling across a planar heterostructure is described by the complex band structure of the barrier. At the $\bar{\Gamma}$ point, the top of the MgS valence band and the bottom of the conduction band are connected by the imaginary band of Δ_1 symmetry. Thus, the lowest decay parameter at the $\bar{\Gamma}$ point will correspond to the states with Δ_1 symmetry, while the Δ_5 is expected to decay much faster.

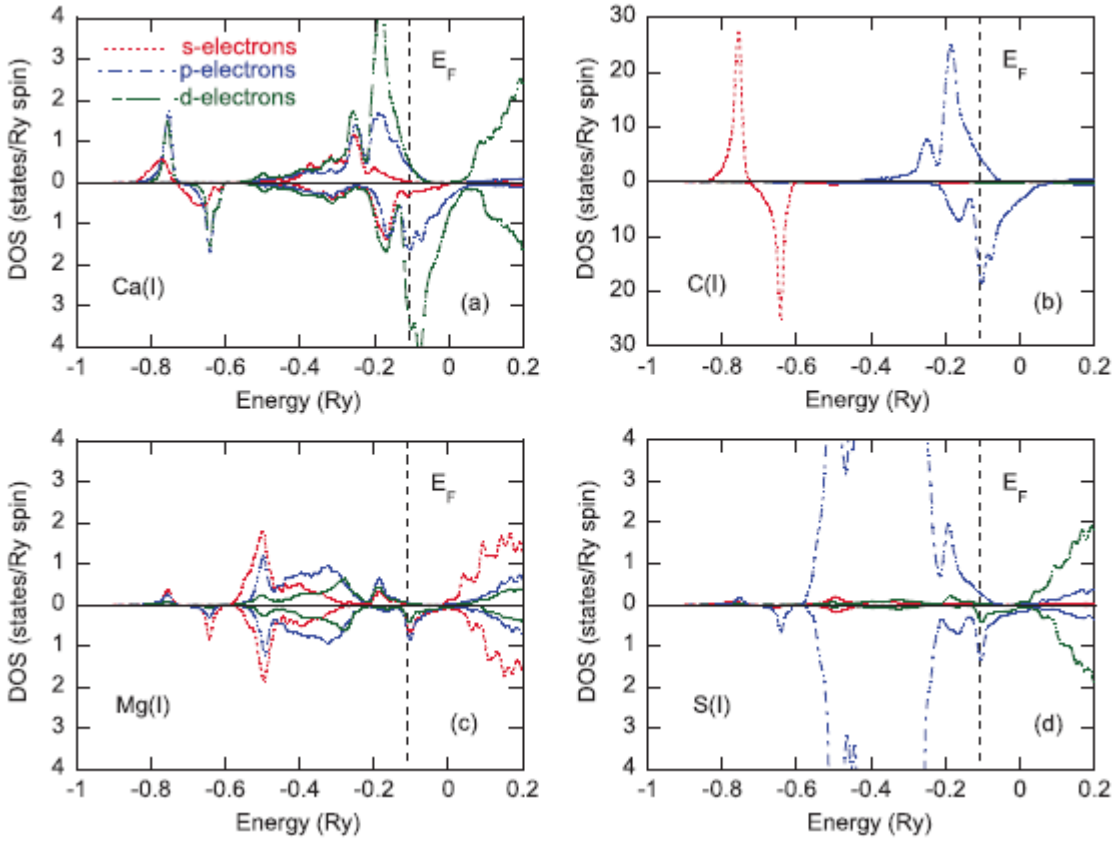

Fig.II.4

The $k_{\|}$ spin-resolved FM and AFM conductances of 2Cu/5CaC/5MgS/5VCaC/3Ca(001) junctions are presented in Fig.II.5. The majority-spin FM conductance is mostly free-electron-like with a smooth peak at the $\bar{\Gamma}$ point and ring-like feature surrounding it, related to Ca-d_{z^2} orbitals. The minority spin FM sub-band also present a peak at the $\mathbf{k}_{\|} = 0$ point, as well as a ring-like feature around it. These channels correspond to the Δ_1 states of CaC electrodes that couple with the slowest decaying Δ_1 states in the MgS barrier. In both spin channels small contributions of Δ_5 states are observed.

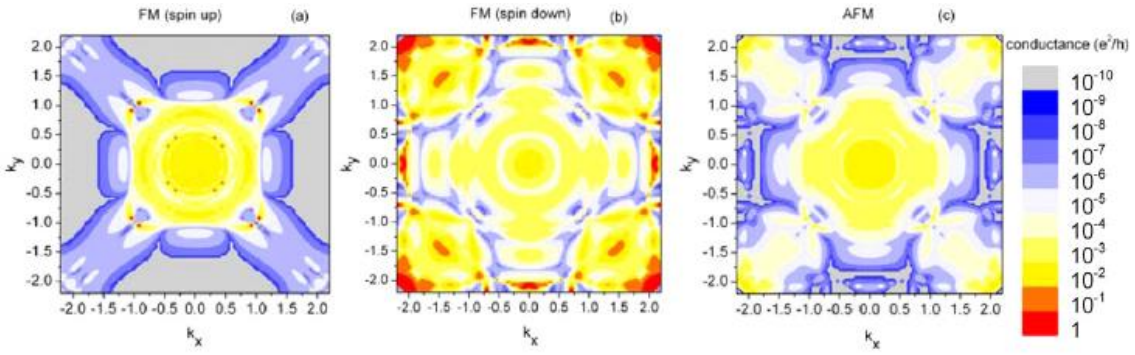

Fig.II.5

The current spin-polarization reaches values as high as 99 %. Very large magnetoresistance ratios, above 10^4 % are evidenced. The highly magnetoresistive effect observed for CaC/MgS/CaC(001) heterojunctions, together with the robust ferromagnetism of CaC(001) electrodes, make this system attractive in context of spin electronics.

The scientific results obtained in the study of CaC/MgS/CaC(001) heterojunctions were published in the paper:

Spin-polarized transport using d^o ferromagnetism: and ab initio study of CaC/MgS/CaC(001) heterojunctions

P.Vlaic, E.Burzo, K.Carva

J. Phys. D.: Appl. Phys. 48, 455002, 2015 IF = 2.721

II.2 Fe/NaBr/Fe interfaces

The NaBr crystallizes in B1(NaCl)-type structure having a lattice parameter a = 5.997352 Å. The iron has bcc-type structure with a = 2.856 Å. Thus, NaBr(001) interfaces epitaxially much in-plane Fe(001) c(2x2) structure, the lattice mismatch being of 4.3 %. NaBr is a wide band gap semiconductor with an experimentally band gap of 7.1 eV. Band structure calculation evidenced somewhat smaller band gap. Thus Fe/NaBr/Fe are MTJ feasible heterostructure for spintronic applications.

By using the interface structure given in Fig.II.6 we analysed the interface stability. The results are close to those evidenced in Fe/LiBr/Fe heterostructures, as discussed in section II.1.

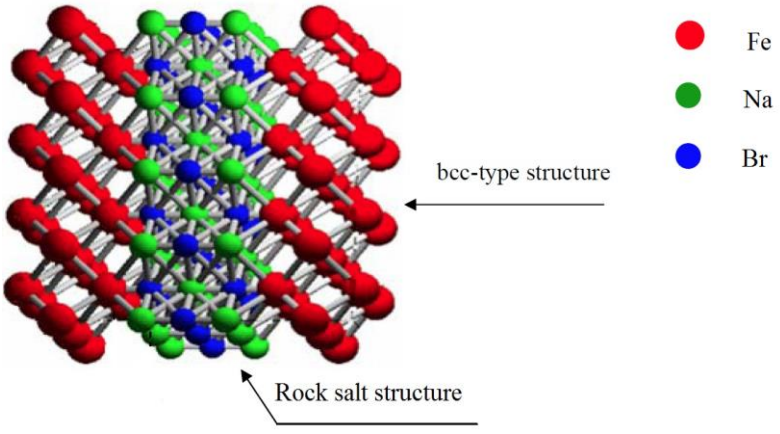

Fig.II.6

III. Double perovskites based on calcium

III.1 The structural and magnetic properties of $Ca_{1.5}La_{0.5}FeMoO_6$ perovskite at high pressure.

The double perovskite oxides of general formula $A_2BB'O_6$, where A is a divalent alkaline earth ion and B or B' are the transition metal ions show interesting magnetic and transport properties, with potential applications in magnetic tunnel junctions.

In order to obtain usefull information on the crystal structures and magnetic properties of perovskites, the system where A = $Ca_{1.5}La_{0.5}$ and B or B' sites contain a mixture of Fe and Mo ions has been studied.

The room temperature XRD pattern shows that $Ca_{1.5}La_{0.5}FeMoO_6$ perovskite crystallizes in a monoclinic $P2_1/n$-type structure. The above structure type is stable in the pressure range $p \leq 5.7$ GPa. The monoclinic β angles are close to 90°, indicating a nearly orthorhombic type lattice. The c and b lattice parameters are more compressible than the a ones. A high decrease of the lattice constants has been shown at p = 1.8 GPa, followed by smaller variations as pressure increases – Fig.III.1. The peculiar pressure behavior of B-Oi and B'-Oi (i = 1,2,3) bond distances shows a complex lattice compression. These features can be evidenced particularly by analysing the evolution with pressure of the distortion index. The distortion index of BO_6 octahedra, $\Delta_d(B)$, increases noticeably with pressure, while that of $B'O_6$= ones shows a less pronounced tendency to decrease. The octahedral tilting angles, in the basal plane, are θi = 12.7° and 15.45° and in apical direction of 8.65°. The corresponding tilting behavior is denoted by $a^-a^-b^+$ [3.1] and is characteristic for $P2_1/n$ type structure. The tilting angles in basal plane increase with pressure.

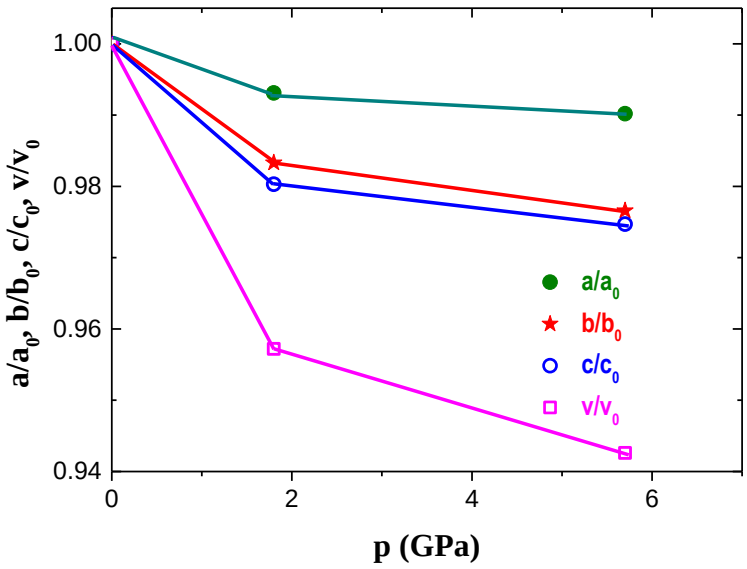

Fig.III.1

The mean valences of cations residing in A dodecahedron and in B or B' octahedra were evaluated using bond- valence-bond length correlations [3.2]. Values of 2.18e^-, 3.37e^- and 4,42 e^- were obtained for cations residing in A, B and B' sites, respectively. Their sum is 12,08 e^-, near the same as expected by the presence of $6O^{2-}$. A high content of Mo ions located in B sites and iron in B' site, respectively is suggested by the above data.

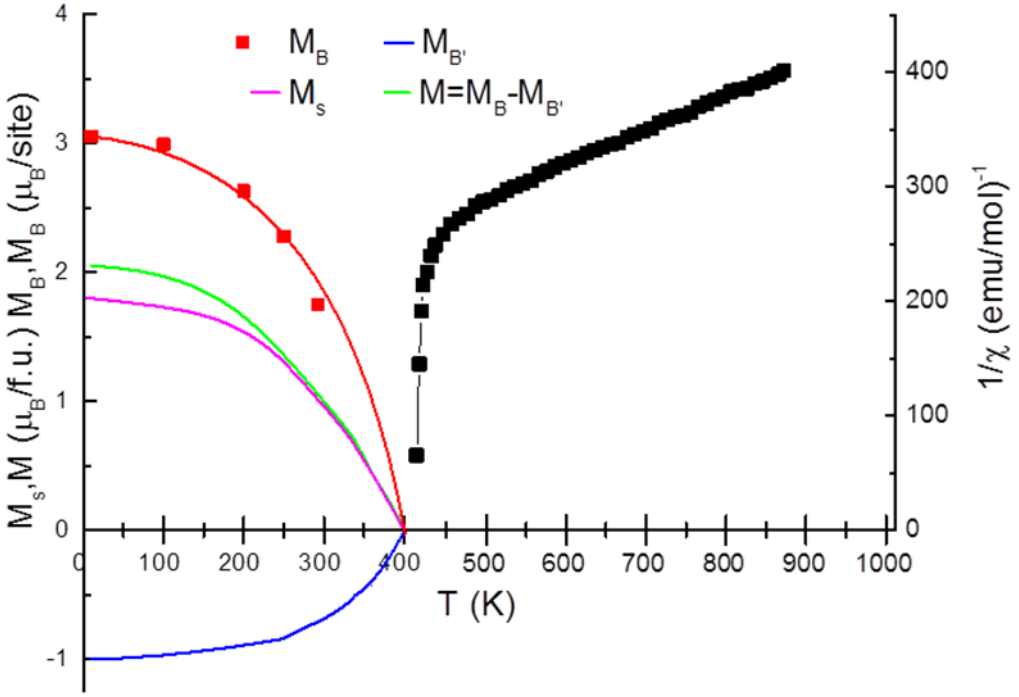

Fig.III.2

The magnetic measurements, at normal pressure, suggest the presence of a small cluster glass contribution, superposed on essentially ferrimangnetic type ordering. The temperature dependence of the magnetic susceptibility, is non linear, characteristic for a ferrimagnetic type ordering – Fig.III.2. Starting from a two magnetic sublattices model, the parameters characterizing the exchange interactions inside and between magnetic sublattices were determined ($J_{BB'}$=-284, $J_{B'B'}$ =103 şi J_{BB} = -88). The presence of a cluster glass is emphasized by the negative mean exchange parameters inside of the one sublattice.

The temperature dependences of the magnetic moments, determined at B site, by neutron diffraction, at different pressures, are given in Fig.III.3.The Curie temperatures increase with a rate of 8.42 K GPa^{-1}. The magnetic moments at T = 10 K, at B site, increase with pressure, particularly at p = 1.8 GPa, while those at B' sites remain nearly constant. The above behavior has been attributed to changes of the cations valence states, as effect of pressure. The increase of the valence from Fe^{2+} to Fe^{3+} is associated with a reduction of ionic radius from 0.78 Å to 0.645 Å, facilitated by lattice compression. In order to keep the charge neutrality an equivalent number of Mo^{6+} ions must to change the valence at Mo^{5+}, the last ion having a greater ionic radius (0.61 Å) than Mo^{6+} (0.59 Å). As a result, the magnetic moments of iron will increase by 1 μ_B/atom while those of Mo^{5+} by 0.35 μ_B/atom. Since the initial fraction of Mo^{6+} is of 35

%, the total increase of the iron moments can by of ≅ 0.35 μ_B, while those of molybdenum ions of ≅ 0.11 μ_B.

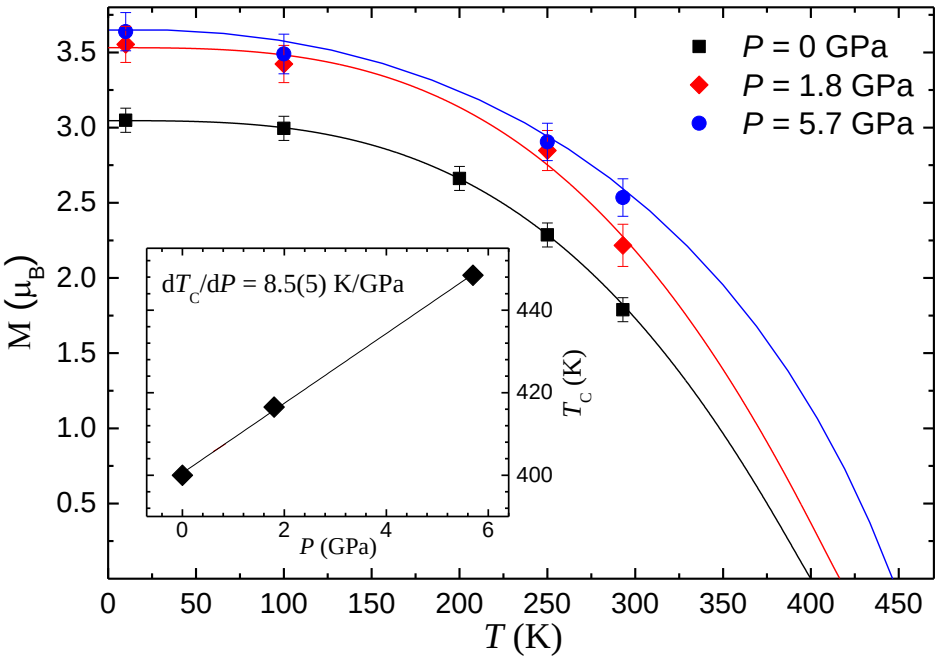

Fig.III.3

Starting from the distributions of cations in B and B' sites and valence states, as suggested by magnetic measurements and bond valence calculations, their populations have been estimated at p = 0 GPa:

B (40 % Fe^{2+}, 30 % Fe^{3+}, 20 % Mo^{5+} și 10 % Mo^{6+})

B' (30 % Fe^{2+}, 45 % Mo^{5+} și 25 % Mo^{6+})

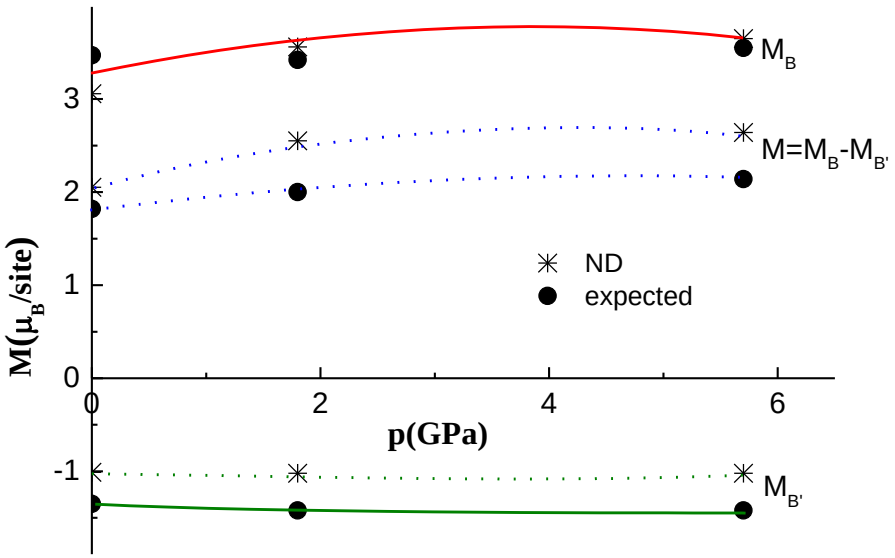

Fig.III.4

The resultant magnetic moments were 3.17 μ_B and mean valence v = 3.30 e^- at B site and 1.35 μ_B and v = 4.35 e^- at B' one, values rather close to experimental data or computed valences. When increasing pressure, according to changes in cations valences, the obtained values describe well the experimentally determined moments as well as the mean cations valences – Fig.III.4.

The increase of the mean B magnetic moment, in parallel with the changes in cations radii, influences the pressure evolution of crystal parameters, particularly at p = 1.8 GPa. At p = 5.7 GPa, there is a only a small additional increase of the magnetic moment (0.09 μ_B), the associated dimensional effects being rather small. The model describes well the pressure dependence of B-Oi and B'-Oi bond distances and distortion index, when considering changes of the mean ionic radius B and B' sites.

III.2 Crystal structures, magnetic and transport properties of calcium based perovskites

The $Ca_2Fe_{1-x}Ni_xMoO_6$ perovskites, with $x \leq 0.2$, were prepared by solid state reaction. These crystallize in a monoclinic type structure having space group $P2_1/n$. The lattice parameters increase as Ni content is higher.

The magnetization isotherms, at 4 K, are given in Fig.III.5. At relative high fields (H > 25 kOe), the magnetizations are saturated. The magnetizations, in the composition range $0 \leq x \leq 0.2$, decrease by ≅ 0.13 μ_B, corresponding to 0.65 μ_B per substituted nickel atom. The thermal variations of Ca_2FeMoO_6 magnetization and of reciprocal susceptibility are given in Fig.III.6. The presence of a ferrimagnetic type ordering is confirmed also by a non-linear temperature dependence of the magnetic susceptibility. Starting from the Curie constant and considering an ionic model, the content of ferrous ions has been estimated at ≅ 60 %. The distribution of Fe and Mo ions in B and B' sites were determined as to fit the saturation magnetization, at 4 K. The Ni^{2+} ions were shown to be distributed both in B and B' sites. The magnetic behavior of Ca_2FeMoO_6 is essentially determined by that of B sublattice.

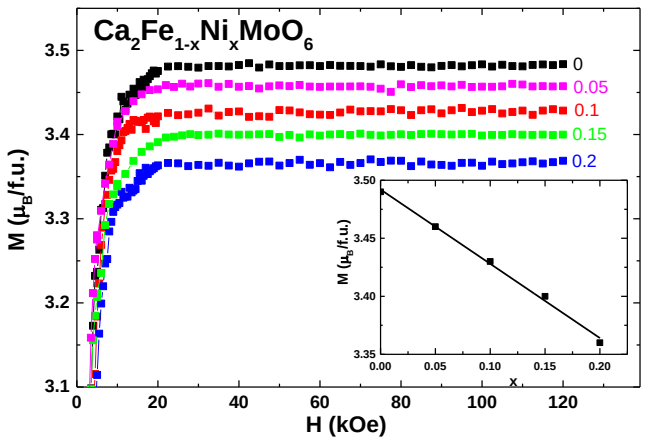

Fig.III.5

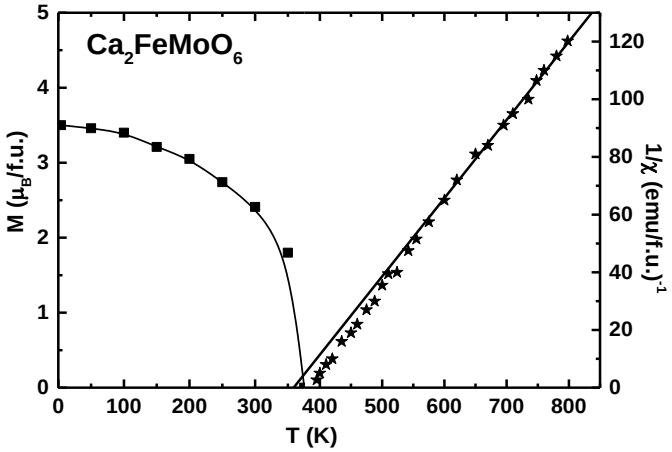

Fig.III.6

The $Ca_2Fe_{1-x}Ni_xMoO_6$ perovskites show a metallic behavior in the temperature range 10 K ≤ T ≤ 300 K. The resisitivities increase, as iron is gradually replaced by nickel, mainly by increasing the number of Ni^{2+}-Mo^{6+} pairs.

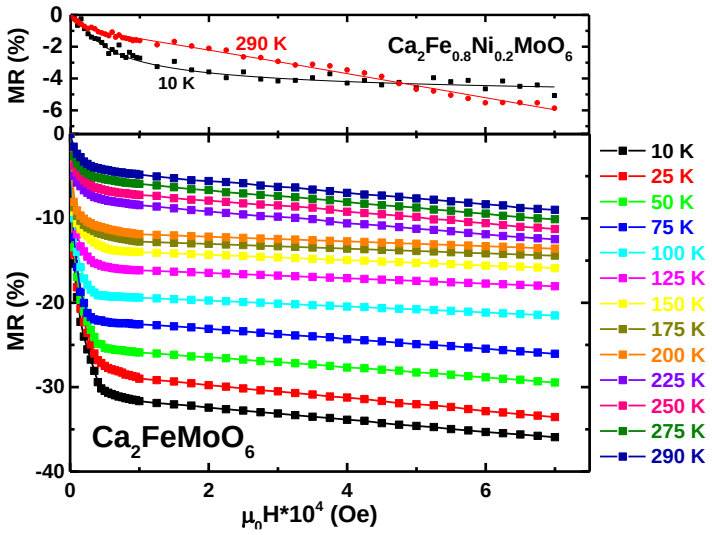

Fig.III.7

The temperature and field dependences of the magnetoresistivities, MR, for $Ca_2Fe_{1-x}Ni_xMoO_6$ samples with x = 0 and 0.2 are given in Fig.III.7. Values of ≅ 36 % and 9 % were determined in field of 70 kOe, for the sample with x = 0, at 10 K and 298 K, respectively. The MR values decrease sensitively when iron is gradually replaced by Ni.

The magnetoresistivities were shown to be determined by both the intergrain tunneling contribution as well as the intergrain one, as described by the relation:

$MR = -P^2m(H)^2[1+P^2m(H)^2]^{-1}-bH$

where P is the degree of spin polarization and m(H) describes the field dependences of the reduced magnetization, in the region near grain boundary, $m(H)=(1-aH^{-1/2})$.

The above relation describes well the experimental MR data. The spin polarization of Ca_2FeMoO_6, at T = 10 K, P=41 %, decreases linearly with temperature. The spin polarization diminishes also when nickel content is higher.

References:

3.1 A.M.Glazer, Acta Cryst. B28, 3384 (1972)

3.2 I.D.Brown, Chem. Rev. 109, 6858 (2009)

III.3 The following papers were published, accepted or sent for publication in 2015 year or presented at International Conferences:

3.1 **E.Burzo, I.Balasz,** M.Valeanu, D.P.Kozlenko, G.E.Kichanov, A.V.Rutkauskas, B.N.Savenko

Magnetic and trasport properties of $Ca_{1.5}La_{0.5}FeMo_{1-x}W_xO_6$ perovskites

Journal of Alloys and Compounds 621, 71-77 (2015) FI = 2.99

3.2 **E.Burzo, I.Balasz**

Crystal structures, magnetic and trasport properties of calcium based perovskites

AIP Conf. Proc. (accepted for publications)

3.3 **E.Burzo,** D.P.Kozlenko, N.T.Dang, S.E.Kichanov, N.O.Golosova

Structural and magnetic properties of $Ca_{1,5}La_{0,5}FeMoO_6$ perovskite at high pressure

Journal of Alloys and Compounds (sent for publications)

International Conferences

3.4 **E.Burzo**

Crystal structures, magnetic and trasport proeprties of calcium based perovskites

BPU-9 International Conference, Istanbul, 24-27.08.2015

Oral presentation, paper O6-OP-13 p.148

3.5 **I. Balasz-Muresan, A.A.Fărcas, E.Burzo**

Magnetic and electrical proeprties of $Ca_2Fe_{1-x}Ni_xMoO_6$ double perovskites

The 15th International Balkan Workshop on Applied Physics, 2-4 July 2015, Poster paper SI P35 p.

IV. Sequential cobalt magnetization collapse in $ErCo_2$

In addition to the objectives of working plan for 2015 year, we studied also the peculiar magnetic properties of $ErCo_2$ compound at high pressures. Starting from these data, the validity of the induced magnetism (epamagnetism) model [4.1] has been confirmed. The model of itinerant electron metamagnetism, generally accepted in literature, cannot describe the observed behavior.

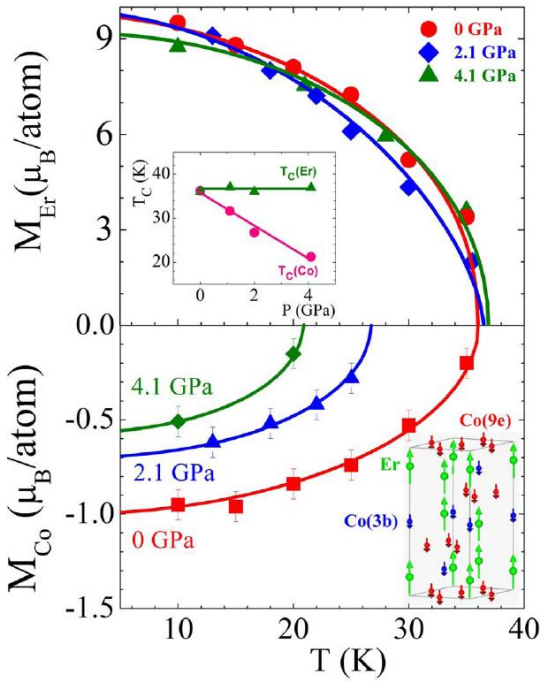

Fig.IV.1

The neutron diffraction studies on $ErCo_2$, at different pressures, evidenced that the magnetizations of Er and Co sublattices become uncoupled under pressure and the ordered Co magnetic moment collapses in the background of nearly unchanged ordered Er magnetic moment – Fig.IV.1. Band structure calculations showed that the cobalt moment is dependent on the exchange field, proportional to exchange splitting of 3d band. No changes in the populations of the cobalt sub-bands was evidenced, as required by the collective electron metamagnetism model – FigIV.2.

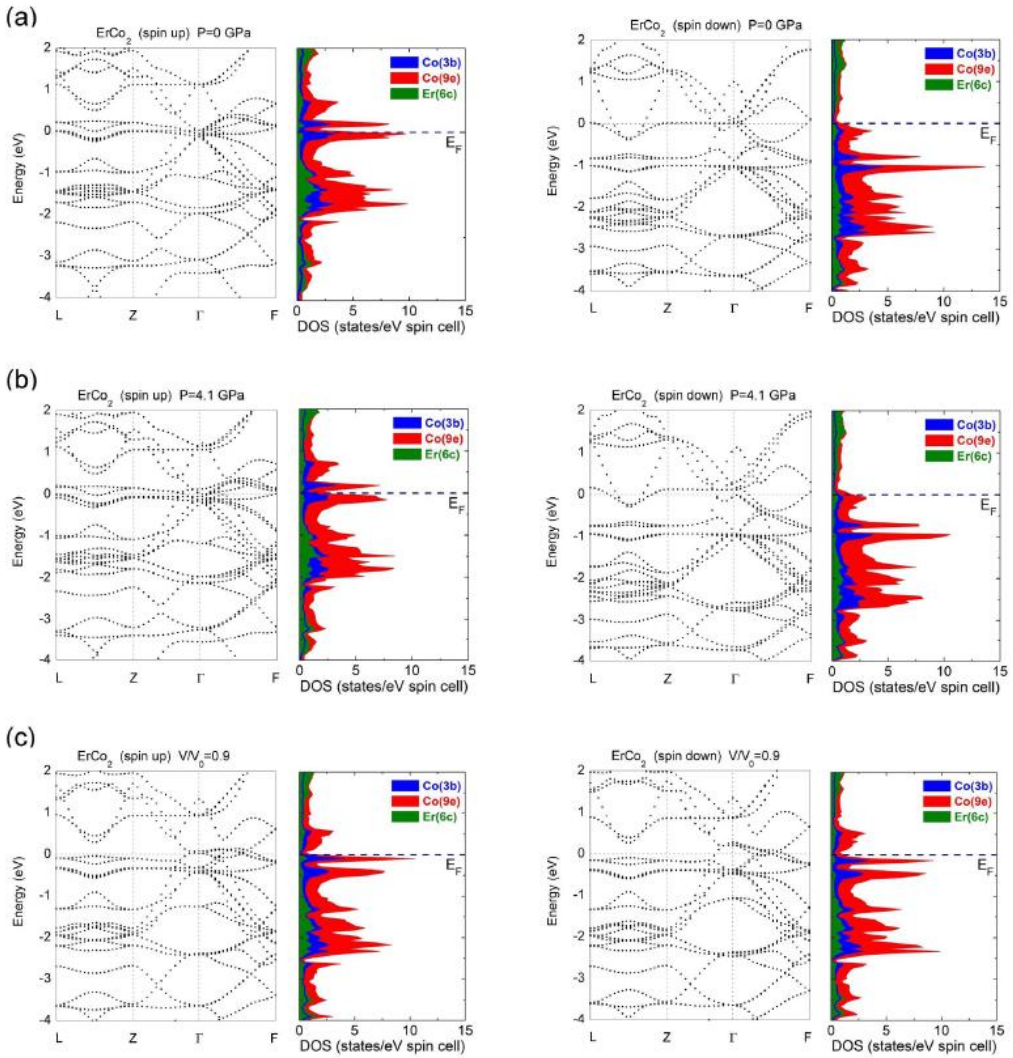

Fig.IV.2

Reference

4.1 **E.Burzo**, J. Less Common Met. 77, 251 (1981), Solid State Commun. 20, 569 (1976)

The paper was published in Scientific Reports (Nature journal)

Sequential cobalt magnetization collapse in $ErCo_2$: beyond the limits of itinerant electron metamagnetism

D.P.Kozlenko, **E.Burzo, P.Vlaic**, S.E.Koichanov, A.V.Rutkauskas, B.N.Savenko,

Scientific Reports 5, 8620 (2015) IF = 5.62.

V. Paper published in 2015 year

1. ***"Oscillatory exchnage coupling and strong direct tunneling in AgCl based heterojunctions"***

   P.Vlaic, E.Burzo, K.Carva

   J.Alloys Comp. 630, 299-309 (2015) IF=2.99

2. ***"Spin-polarized transport using d^o ferromagnetism: and ab initio study of CaC/MgS/CaC(001) heterojunctions"***

   P.Vlaic, E.Burzo, K.Carva

   J. Phys. D.: Appl. Phys. 48, 455002-455010, 2015 IF = 2,721

3. ***"Magnetic and trasport properties of $Ca_{1.5}La_{0.5}FeMo_{1-x}W_xO_6$ perovskites"***

   E.Burzo, I.Balasz, M.Valeanu, D.P.Kozlenko, G.E.Kichanov, A.V.Rutkauskas, B.N.Savenko

   Journal of Alloys and Compounds 621, 71-77 (2015) IF = 2.99

4. ***"Pressure effects on the magnetic behaviour of cobalt in rare-earth compounds"***

   E.Burzo, P.Vlaic, D.P.Kozlenko

   Rom. J.Phys. 60, 200 (2015) IF=0.92

Papers accepted or sent for publications

5. ***"Crystal structures, magnetic and transport properties of calcium based perovskite"***

   E.Burzo, I.Balasz

   AIP Conf. Proc. (accepted)

6. ***"Structural and magnetic properties of $Ca_{1,5}La_{0,5}FeMoO_6$ perovskite at high pressure"***

   E.Burzo, D.P.Kozlenko, N.T.Dang, S.E.Kichanov, N.O.Galosova

   Journal of Alloys and Compunds IF=2.99

7. ***Are insulating LiF barriers relevant for spin-polarized tunneling applications? Insight from first-principles***

   E.Burzo, P.Vlaic, K.Carva

   Journal Phys.D:Appl. Phys. (sent for publication) IF = 2,721

Papers presented at International Conferences

1. ***"Crystal structures, magnetic and transport properties of calcium based perovskites"***

   E.Burzo

   BPU-9 International Conference, Istanbul 24-27.08.2015

   Oral presentation, paper 06-OP-13 p.148

2. ***"Electronic properties of Fe/LiF(LiBr)/Fe magnetic tunnel junctions"***

   E.Burzo, P.Vlaic

   Invited lecture, The 15th International Balkan Workshop on Applied Physics, 2-4 July 2015, pages SO-02 p.15

3. ***"Magnetic and electrical properties of $Ca_2Fe_{1-x}Ni_xMoO_6$ double perovskite"***

I.Balasz-Muresan, A.Fărcas, E.Burzo

Poster paper, The 15th International Balkan Workshop on Applied Physics, 2-4 July 2015 paper SI p.35 p.63

Paper published in addition to the main topics

"Sequential cobalt magnetization collapse in $ErCo_2$: beyond the limits of itinerant electron metamagnetism"

D.P.Kozlenko, **E.Burzo, P.Vlaic**, S.E.Koichanov, A.V.Rutkauskas, B.N.Savenko,

Scientific Reports (UK) 5, 8620 (2015) IF = 5.578.

Project Manager,

Acad. Prof. dr. Emil Burzo